

Detection of H₂ in the TWA 7 System: A Probable Circumstellar Origin

LAURA FLAGG,¹ CHRISTOPHER M. JOHNS-KRULL,¹ KEVIN FRANCE,² GREGORY HERCZEG,³ JOAN NAJITA,⁴
JOHN M. CARPENTER,⁵ AND SCOTT J. KENYON⁶

¹*Department of Physics and Astronomy, Rice University, 6100 Main St. MS-108, Houston, TX 77005, USA*

²*Laboratory for Atmospheric and Space Physics, University of Colorado, 600 UCB, Boulder, CO 80309, USA*

³*Kauli Institute for Astronomy and Astrophysics, Peking University, Yi He Yuan Lu 5, Haidian Qu, Beijing 100871, China*

⁴*National Optical Astronomy Observatory, 950 Cherry Avenue, Tucson, AZ. 85719, USA*

⁵*Joint ALMA Observatory, Avenida Alonso de Córdova 3170, Santiago, Chile*

⁶*Smithsonian Astrophysical Observatory, 60 Garden Street, Cambridge, MA 02138 USA*

ABSTRACT

Using HST-COS FUV spectra, we have discovered warm molecular hydrogen in the TWA 7 system. TWA 7, a ~ 9 Myr old M2.5 star, has a cold debris disk and has previously shown no signs of accretion. Molecular hydrogen is expected to be extremely rare in a debris disk. While molecular hydrogen can be produced in star spots or the lower chromospheres of cool stars such as TWA 7, fluxes from progressions that get pumped by the wings of Ly α indicate that this molecular hydrogen could be circumstellar and thus that TWA 7 is accreting at very low levels and may retain a reservoir of gas in the near circumstellar environment.

Keywords: stars: individual (TWA 7)

1. INTRODUCTION

Planet formation and evolution are heavily dependent on the circumstellar environment. The circumstellar material can dictate formation, composition, orbital parameters, and migration of planets. While much has been learned in recent years about circumstellar disks, especially with ALMA (Andrews et al. 2018), the evolution from protoplanetary disk to debris disk is not well understood. This time period is crucial for the final stages of the growth of terrestrial planets and the early evolution of their atmospheres (e.g. Kenyon & Bromley 2006; Olson & Sharp 2019). Additionally, ALMA typically images only the outer regions of disks; it is also of interest to understand the inner few AU of a system where many exoplanets are found and where the systems' habitable zones are.

Protoplanetary disks consist of gas, dust, and eventually planetesimals. All three components play a crucial role in the formation and evolution of planets. Measurements of micron-sized dust are relatively easy, as dust can produce detectable amounts of infrared (IR) emission, even through the debris disk stage. However, the primordial gas, which is mostly molecular hydrogen, is assumed to be 99% of the protoplanetary disk mass (see review by Williams & Cieza 2011) and controls much of the disk dynamics, such as altering orbits of planetesimals and planets (Weidenschilling 1977; Goldreich & Sari 2003; Youdin & Goodman 2005; Baruteau et al. 2014, e.g.,) and potentially producing rings and spirals (Lyra & Kuchner 2013; Gonzalez et al. 2017). Lower gas fractions and optically thin gas are expected in debris disks (Wyatt 2008), although the precise gas fraction is poorly constrained (Matthews et al. 2014) and possibly varies significantly between disks. But even small amounts of optically thin gas can still have a large effect on disk dynamics (e.g. Takeuchi & Artymowicz 2001; Lyra & Kuchner 2013). Thus, to understand the evolution of the circumstellar environment, we must understand how the hydrogen evolves.

However, H₂ is notoriously hard to detect. Its only allowed electric dipole transitions are in the ultraviolet (UV). In most circumstellar environments, those transitions require excited H₂, which can occur in circumstellar disks with warm gas (Nomura & Millar 2005; Ádámkóvics et al. 2016). Warm gas is common in protoplanetary disks, but is less likely to be found in debris disks because of the generally large distance of the gas from the central star. Chromospheric

and transition region lines, such as Ly α , pump the H₂ molecule from an excited level in the ground electronic state to the first (Lyman) or second (Werner) electronic levels. Because of extremely high oscillator strengths, the excited molecule immediately decays back to the ground electronic level in a fluorescent cascade, emitting photons. The set of emission lines produced by transitions from a single excited electronic state to the multiple allowed ground electronic states is called a progression. Within a given progression, H₂ line fluxes are proportional to their branching ratios (Wood et al. 2002; Herczeg et al. 2004). Because of this, far UV spectra are a powerful way to characterize the warm H₂ gas. Emission from these lines is a probe of gas temperature. But as all these transitions are in the UV, they require data from space-based observatories, thus limiting the number of observations currently available. There are magnetic quadrupole transitions in the IR that have been detected in protoplanetary disks (e.g. Weintraub et al. 2000; Bary et al. 2003); unfortunately, they are weak and require much larger amounts of warm H₂ than debris disks typically have in order to detect them (e.g. Bitner et al. 2008; Carmona et al. 2008).

To try to get around these issues, other molecules, most notably IR and millimeter transitions of HD and more commonly CO, have been used to trace the H₂ (e.g. Trapman et al. 2017). However, neither is a perfect tracer, and both rely on an assumed ratio to H₂. For example, disk mass estimates have often used the ISM CO/H₂ of $\sim 10^{-4}$, consistent with the value found by France et al. (2014) based on CO and H₂ observations in the UV, but other recent studies have shown that CO appears depleted in protoplanetary disks (Favre et al. 2013; Schwarz et al. 2019; McClure 2019). Furthermore, the difference in chemistry and masses between the molecular species mean that neither HD or especially CO trace H₂ perfectly (Molyarova et al. 2017; Aikawa et al. 2018).

Molecular hydrogen emission has been detected in every protoplanetary and transition disk that have far UV spectral observations (e.g. Valenti et al. 2000; Ardila et al. 2002; Herczeg et al. 2006; Ingleby et al. 2009; France et al. 2012; Yang et al. 2012; France et al. 2017). Debris disks are not defined by their gas content — they are instead defined by secondary dust produced from planetesimal collisions, which observationally gets translated into a fractional luminosity, $f = L_{disk}/L_*$ less than 10^{-2} — but all evidence indicates that compared with protoplanetary disks, they have a smaller gas-to-dust ratio and less gas in total (e.g. Chen et al. 2007). Other gas species, like CO, have been detected in debris disks (e.g. Roberge & Weinberger 2008; Moór et al. 2011; Dent et al. 2014; Higuchi et al. 2017), but the only previous potential detection of H₂ in what is clearly a debris disk is from AU Mic (France et al. 2007). This is not unexpected. While comets in our own Solar System produce CO, they do not produce H₂ (Mumma & Charnley 2011). Thus, it is likely that secondary H₂ is not produced in the same manner as secondary CO. In several cases, there are arguments for the reclassification of systems based on the discovery of H₂, such as RECX 11 (Ingleby et al. 2011a), HD 98800 B (TWA 4 B) (Yang et al. 2012; Ribas et al. 2018), and potentially DoAr 21 (Bary et al. 2003; Jensen et al. 2009). But exactly when and on what timescale the H₂ dissipates is not known.

Since even small amounts of H₂ gas can have a significant impact on planetary systems at ages ~ 10 Myr, we have begun a program to examine UV spectra of young stars that show no evidence of near-infrared (NIR) excess. One specific way that gas can impact a system is by limiting the IR flux from dust produced by planetesimal collisions. Kenyon et al. (2016) show that there is a discrepancy between the incidence rate of dust expected to be produced by terrestrial planet formation (2 to 3% of young systems) and the incidence rate of close-in terrestrial planets (20% of mature systems). Gas, however, could sweep away that dust via gas drag, making it harder to detect. Thus, it is critical to understand the evolution of H₂ in the terrestrial planet forming regions.

2. TARGET AND OBSERVATIONS

TWA 7 is an M dwarf that is part of the ~ 7 -10 Myr TW Hya Association (Webb et al. 1999). Recent spectral classifications assign an M2 or M3 spectral type (Manara et al. 2013; Herczeg & Hillenbrand 2014); we adopt M2.5. The star is surrounded by a debris disk that was first detected due to its IR excess at 24 and 70 μm by Low et al. (2005) with the Spitzer Space Telescope. However, the lack of near IR excess (Weinberger et al. 2004) and typical accretion signatures (Jayawardhana et al. 2006) strongly imply that it is a “cool” debris disk, making it one of the few known M stars with a debris disk (Theissen & West 2014). The dust in the disk has since been detected in the FIR at 450 and 850 μm using the James Clerk Maxwell Telescope (Matthews et al. 2007) and at 70, 160, 250, and 350 μm using the Herschel Space Observatory (Cieza et al. 2013). No [O I] was detected by Herschel at 63 μm (Riviere-Marichalar et al. 2013), but CO has been recently detected using ALMA in the J=3-2 transition (Matrà et al. 2019). The disk has been imaged in the IR with SPHERE showing spiral arms near 25 AU (Olofsson et al. 2018). Yang et al. (2012) and France et al. (2012) both failed to detect H₂ around TWA 7 in UV spectra. Yang et al. (2012) used a less sensitive

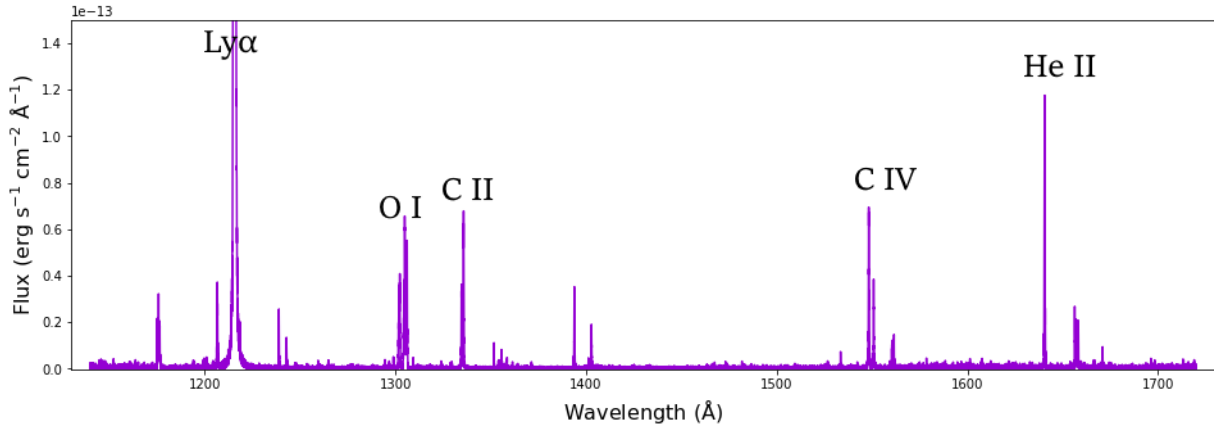


Figure 1. The spectrum of TWA 7 used for analysis with the most prominent stellar features labeled. Note that the Ly α profile is largely geocoronal airglow emission and was thus not used.

prism spectrum; France et al. (2012) looked at 12 H₂ features separately, as opposed to detecting the combined H₂ emission from many features as we do in this paper. (See Section 3.1.)

We can put some constraints on the expected H₂ based on dust and CO measurements. For TWA 7, the total dust mass in the disk, M_d , is $2 \times 10^{-2} M_{\oplus}$ (Bayo et al. 2019), while the mass of CO in the disk, M_{CO} , is $0.8\text{--}80 \times 10^{-6} M_{\oplus}$ (Matrà et al. 2019). Based on these estimates, if TWA 7 has an ISM value for the CO/H₂ ratio of $\sim 10^{-4}$ then we can expect M_{H_2} to be on the order of M_d . If it has a lower CO/H₂ of $\sim 10^{-6}$, as TW Hya has (Favre et al. 2013), we can expect M_{H_2} to be $100\times$ larger than M_d , consistent with the ISM gas-to-dust ratio (Spitzer 1978). Models that have explored gas-to-dust ratios between 0.01 and 100 indicate that gas can significantly influence the disk dynamics (Youdin & Goodman 2005; Lyra & Kuchner 2013; Gonzalez et al. 2017), so in either case, H₂ could play an important if not dominant role in TWA 7’s disk dynamics. Given the presence of this distant reservoir of gas, we explore here the possibility that an (as yet unseen) reservoir of gas is also present at smaller disk radii, in the terrestrial planet region of the disk.

For this work, we use archival HST-Cosmic Origins Spectrograph (COS) observations of TWA 7 from May 2011 (PID 11616, PI: G. Herczeg). The data were acquired with the far UV medium resolution modes of COS: G130M and G160M. These spectra have a spatial resolution of 1” and a wavelength uncertainty ~ 15 km/s (Dashtamirova et al. 2020). The observations are at a range of central wavelengths that allow us to get a contiguous spectrum that spans from 1133 to 1795 Å (Figure 1). In addition to TWA 7, we also analyze spectra of classical T Tauri stars (CTTS) and main sequence M dwarf stars for comparison purposes (Table 1) taken between December 2009 and August 2015. The CTTS were chosen from the stars analyzed by France et al. (2012) that had extinction values measured by both Herczeg & Hillenbrand (2014) and Furlan et al. (2011). The main sequence M dwarfs were from Kruczek et al. (2017), chosen because they had H₂ detected from the stellar photosphere and COS spectra that covered a comparable wavelength range. One of the six M dwarfs — GJ 581 — has a cold, faint debris disk (Lestrade et al. 2012), but it is much older (2–8 Gyr) and less active (Schöfer et al. 2019) than TWA 7 or the CTTS. Its disk is also significantly less luminous than that of TWA 7 (Choquet et al. 2016). The remaining five M dwarfs have no detected disks. All spectra were observed with COS in a similar manner. Spectra were reduced by the CALCOS pipeline. Multiple observations were then co-added into one spectrum as described by Danforth et al. (2016). The TWA 7 spectrum we analyzed is plotted in Figure 1.

We also used archival HST-STIS spectra of TW Hya, reduced with the STIS pipeline. For each observation, we combined the orders to create a single spectrum. We then co-added the observations in a similar manner to the way we co-added the observations from COS.

3. ANALYSIS AND RESULTS

3.1. Methods for Cross-Correlation

In protoplanetary disks and nearby M dwarfs, the strength of the H₂ lines make them clearly detectable above the noise; however, this is not the case for systems with smaller amounts of H₂ flux. Instead, we take advantage of the many weak H₂ lines in the system and use a cross-correlation function (CCF), a technique that has been used

Table 1. Stellar Properties

Object	PID/PI	Distance (pc)	RV (km s ⁻¹)	A _V ^a (mag)	A _V ^b (mag)
TWA 7	11616/Herczeg	34.0	11.4	...	0.00^c
Classical T Tauri Stars					
AA Tau	11616/Herczeg	136.7	17.0	1.9	0.40
BP Tau	12036/Green	128.6	15.2	1.0	0.45
DE Tau	11616/Herczeg	126.9	15.4	0.9	0.35
DM Tau	11616/Herczeg	144.5	18.6	0.0	0.10
DR Tau	11616/Herczeg	194.6	21.1	1.4	0.45
GM Aur	11616/Herczeg	159.0	15.2	0.6	0.30
HN Tau	11616/Herczeg	136.1	4.6	1.0	1.15
LkCa 15	11616/Herczeg	158.2	17.7	1.0	0.30
SU Aur	11616/Herczeg	157.7	14.3	0.9	0.65
UX Tau	11616/Herczeg	139.4	15.5	0.5	0.00 ^c
Main Sequence M Stars with H ₂					
GJ 176	13650/France	9.5	26.2
GJ 832	12464/France	5.0	13.2
GJ 667 C	13650/France	7.2	6.4
GJ 436	13650/France	9.8	9.6
GJ 581	13650/France	6.3	-9.4
GJ 876	12464/France	4.7	-1.6
STIS Spectra					
TW Hya	11608/Calvet	60.1	13.4	...	0.00

NOTE—Properties of stars analyzed in this paper.

^a A_V from [Furlan et al. \(2011\)](#)

^b A_V from [Herczeg & Hillenbrand \(2014\)](#) with uncertainties of 0.15 mag.

^c The measured value was negative. Since this is unphysical, we adapted an extinction of 0.0 mag.

Distances are from ([Bailer-Jones et al. 2018](#)) based on Gaia DR2 [Collaboration et al. \(2018\)](#). RVs of the T Tauri stars are from [Nguyen et al. \(2012\)](#), from Gaia DR2 for the M stars, and from [Torres et al. \(2006\)](#) for TW Hya and TWA 7. Based on extinction measurements from stars in the Local Bubble ([Leroy 1993](#)), we assume these Main Sequence M stars have no extinction.

previously with IR data to study gas in protoplanetary disks ([Hartmann & Kenyon 1987](#)). The CCF allows us to combine the signal from multiple lines into one signal by calculating how well the spectrum correlates with that of a model template ([Tonry & Davis 1979](#)). Our full template was created using the procedure from [McJunkin et al. \(2016\)](#) for a temperature of 2500 K and a column density of $\log N(\text{H}_2)=19 \text{ cm}^2$. As temperature and density have little effect on the relative strengths of these lines in protoplanetary disks ([France et al. 2012](#)), we used the same template for all the stars. Ly α also has a significant impact on H₂ line strengths, but its profile is contaminated from self-absorption, ISM absorption, and geocoronal airglow, and thus cannot be used for all of our targets. As a result, we do not consider the shape of the Ly α profile when defining our template. We use a single FWHM of 0.047 Å for

Table 2. Progressions Analyzed

$[v', J']$	λ_{pump} (Å)	velocity (km s ⁻¹)	TW Hya H ₂ Flux (10 ⁻¹⁵ erg cm ⁻² s ⁻¹)	oscillator strength (× 10 ⁻³)	$[v'', J'']$	E'' (eV)
[3, 13]	1213.356	-571	4.7	20.6	[1,14]	1.79
[4, 13]	1213.677	-491	2.4	9.33	[2,12]	1.93
[3, 16]	1214.465	-297	14.9	23.6	[1,15]	1.94
[4, 4]	1214.781	-219	8.9	9.90	[3,5]	1.65
[1, 7]	1215.726	14	16.2	34.8	[2,6]	1.27
[1, 4]	1216.070	99	36.0	28.9	[2,5]	1.20
[3, 0]	1217.038	338	3.5	1.28	[3,1]	1.50
[0, 1]	1217.205	379	37.9	44.0	[2,0]	1.00
[0, 2]	1217.643	487	33.4	28.9	[2,1]	1.02
[2, 12]	1217.904	551	18.4	19.2	[1,13]	1.64
[2, 15]	1218.521	704	3.1	18.0	[1,14]	1.79
[0, 3]	1219.089	844	2.1	25.5	[2,2]	1.04

NOTE—Velocity is from Ly α center. TW Hya H₂ Flux as measured by [Herczeg et al. \(2006\)](#).

Oscillator strengths of the pumping transitions calculated by [Herczeg et al. \(2006\)](#) based on [Abgrall et al. \(1993\)](#).

$[v'', J'']$ and E'' are the lower level in the electronic ground state for the pumping transition and the corresponding energy for that state.

Each of these progressions is pumped by Ly α flux and can decay to multiple lower states, resulting in a set of H₂ emission lines throughout the UV.

the lines in the template, chosen solely because it is the width that maximizes the CCF for TWA 7. Templates for individual progressions were created by picking the lines from the full template based on [Abgrall et al. \(1993\)](#) (Figure 2). Although there are many H₂ lines, focusing only on the strongest lines gives the clearest signal. We chose the minimum H₂ line strength in the template that maximized the CCF detection for TWA 7 for each progression. The minimum line strength is dependent on how strong the lines in that progression are: progressions with weaker fluxes require smaller minimum line strengths. While we analyzed 12 different progressions (Table 2), chosen because all 12 were detected by [France et al. \(2012\)](#) in protoplanetary disks, our analysis focused on the progressions that typically produce the most H₂ flux in CTTS — [1,4], [1,7], [0,1], and [0,2]. Each of these progressions is excited by Ly α and can decay to multiple lower states, resulting in a set of H₂ emission lines throughout the UV. The total summed flux in an individual progression is a function of having enough Ly α photons to pump the H₂ molecule to the excited state (Figure 3), the filling factor of H₂ around the Ly α , the column density in the excited rovibrational level of the X electronic state, and the oscillator strength of the the pump transition ([Herczeg et al. 2006](#)).

Since we want to be sure that we are only cross-correlating continuum and H₂ emission (plus the associated noise) and not emission from hot gas lines from the chromosphere or transition region, we masked out FUV lines commonly seen in lower mass stars from [Herczeg et al. \(2002\)](#), [Brandt et al. \(2001\)](#), and [Ayres \(2015\)](#). As these lines have different widths in different stars depending on numerous properties, we erred on the side of masking the wavelength regions covered by the broadest of these features to minimize the chance of a false positive from a line that was not H₂.

Cross-correlating the entire spectrum with the entire masked template returns a tentative detection. However, this involves cross-correlating a significant amount of noise which can weaken the detection. Therefore we created segments of spectrum for each H₂ feature of ~ 1 Å (~ 200 km/s) wide centered around the wavelengths of expected H₂ lines, which is wide enough to get the entire line profile without adding too much continuum flux or noise. (We cannot be certain as to whether the photons detected outside of lines are from the star itself, as M dwarfs have very little stellar continuum flux in these regions, so we will refer to the region outside of lines as “continuum/noise.”) To calculate the final CCF, we explored two procedures to verify any findings. With both methods, if the flux for every line is emitted at a similar relative velocity (within ~ 10 km s⁻¹), the CCF’s signal will grow stronger. In the first method, we created one long spectrum by putting all the individual segments end-to-end. We do the same for the corresponding template

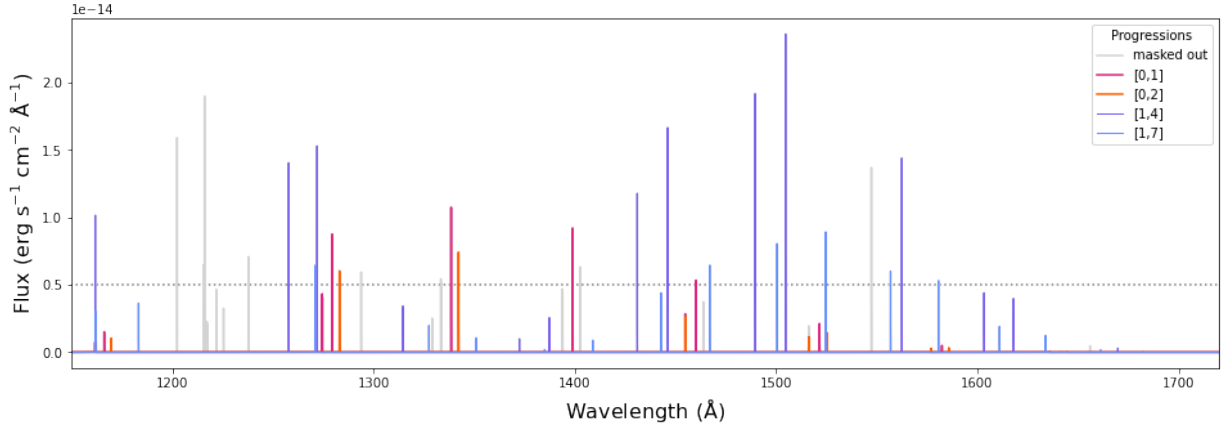


Figure 2. Templates of the most prominent progressions used for cross-correlation. A cutoff for a minimum line strength of $5 \times 10^{-15} \text{ erg s}^{-1} \text{ cm}^{-2} \text{ \AA}^{-1}$ is also shown.

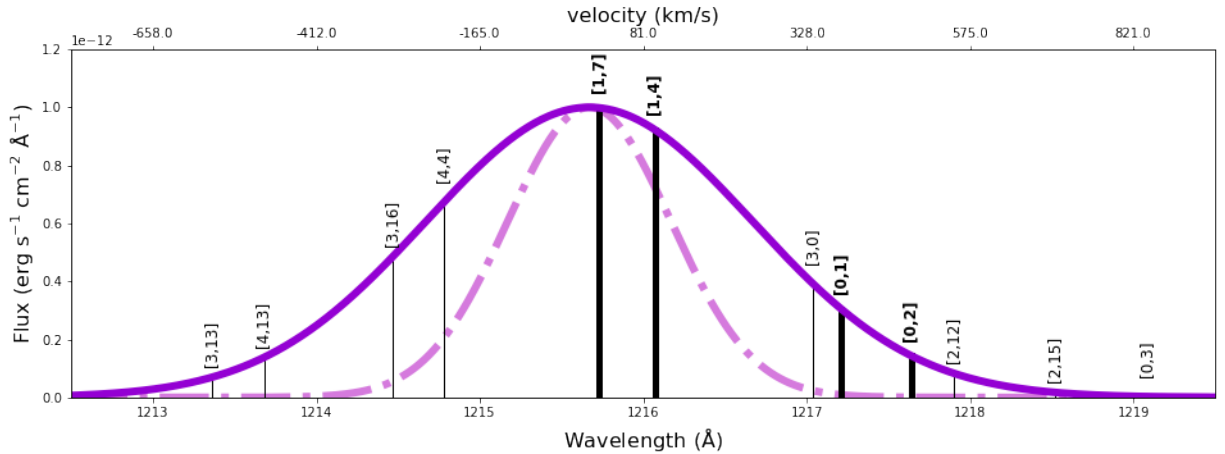


Figure 3. Schematic Ly α profiles. The solid purple line corresponds to a broader profile, like seen with CTTS, while the dashed pink line is indicative of Main Sequence stars with a more narrow profile. The pumping wavelengths of some prominent are marked. The strongest progressions have not only substantial Ly α flux but also larger oscillator strengths and smaller lower state energies (Table 2).

segments. We then cross-correlated this pieced together spectrum with the same regions from the template. In the second method, we cross-correlated each segment of spectrum individually with its corresponding template segment and added the cross-correlation functions. Because of this, we chose to use a CCF that has not been normalized for length, which is usually the last step of calculating the CCF. Unnormalized CCFs work equally well for both of our methods; normalized CCFs of different lengths cannot be added linearly, because longer CCFs should be weighted more.

3.2. H_2 Detection and Verification

We detect peaks near the stellar radial velocity in the CCFs of the spectra of TWA 7 (Figure 4) using a minimum H_2 template line strength cutoff of $5 \times 10^{-15} \text{ erg s}^{-1} \text{ cm}^{-2} \text{ \AA}^{-1}$. The peaks are detected with both methods — segmented spectrum and added CCF — for calculating the CCF. Although the peak is strongest when all of the most prominent progressions are included, we also see significant ($>3\sigma$) detections when some individual progressions are analyzed. While the peak for [0,1]+[0,2] is slightly off-center from the systemic velocity of 11.4 km/s, we attribute this to the uncertainties in the wavelength calibration that can lead to shifts in the resulting velocities by up to 15 km/s, as described in Linsky et al. (2012).

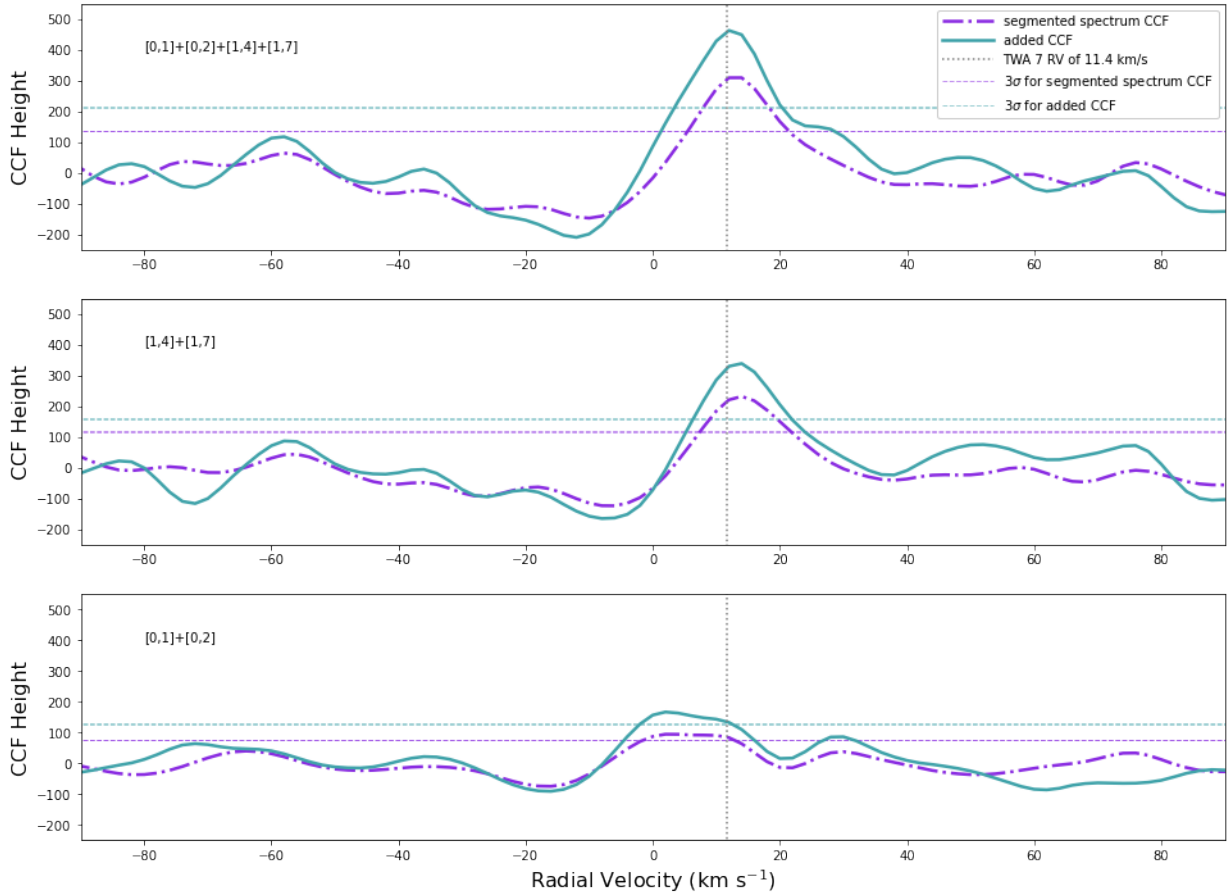


Figure 4. Cross-correlation functions of TWA 7 for the most prominent H₂ progressions.

The strength of the cross-correlation function is dependent on the S/N in the H₂ lines. Since we are trying to measure the height and significance of the CCF peak, we need to understand the noise properties of the observed spectrum. This is made more difficult, because there are so few FUV photons that reach us. For example, [Loyd et al. \(2016\)](#) looked for FUV continuum in our M dwarf sample, obtaining a significant detection for only 3 of 6 targets. As a result, noise in our spectrum cannot be approximated to be Gaussian as it can when there are hundreds or thousands of counts. Typical continuum/noise regions in our TWA 7 spectrum have flux distributions that look approximately like that seen in [Figure 5](#) where we show a histogram of flux levels found in the continuum/noise of TWA 7.

There are several potential issues in modeling this noise. The first is that there are undoubtedly unidentified lines that we do not mask, as possibly seen in the increase around $0.3 \times 10^{-15} \text{ erg s}^{-1} \text{ cm}^{-2} \text{ \AA}^{-1}$. However, since other unidentified lines could possibly overlap with the H₂ lines, we choose not to remove this peak from the distribution. Another issue is that because of the low flux level, when the detector background gets subtracted, we end up measuring “negative” flux in some wavelength bins. To deal with this, we estimate the noise in two separate ways: with a scaled Poisson distribution and using the actual distribution fit with a kernel density estimator (KDE) ([Rosenblatt 1956](#); [Parzen 1962](#)), as shown in [Figure 5](#). The scaled Poisson was determined by calculating the skew of the distribution of continuum/noise, γ_1 . The mean of the Poisson distribution λ is then γ_1^{-2} . We then convert from counts to flux using a constant scaling factor determined by the mean of the distribution. The KDE was calculated with a Gaussian kernel using a bandwidth (equivalent to the sigma parameter) of $10^{-17} \text{ erg s}^{-1} \text{ cm}^{-2} \text{ \AA}^{-1}$. We randomly draw our noise from these distributions. These two noise models cover the range of possibilities of the underlying true noise, so a robust detection will only be evident if it occurs using both noise models.

To determine the significance of the detection, we used our noise models to create spectra containing only noise. We then cross-correlated these noise spectra with the template in the same ways we did for the TWA 7 spectrum. We then record the CCF maximum within 15 km s^{-1} of the systemic velocity. We chose this range, because this was the

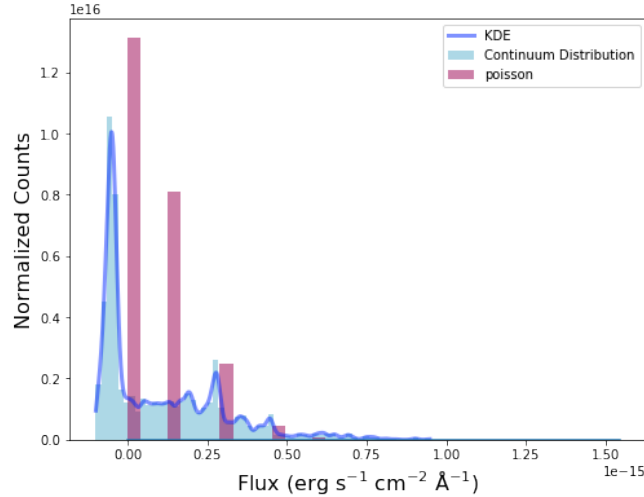


Figure 5. Typical continuum/noise distributions, which we model in two ways: by creating a KDE of the distribution and by scaling a discrete Poisson distribution to the data. Both were normalized so that the total area is equal to 1.

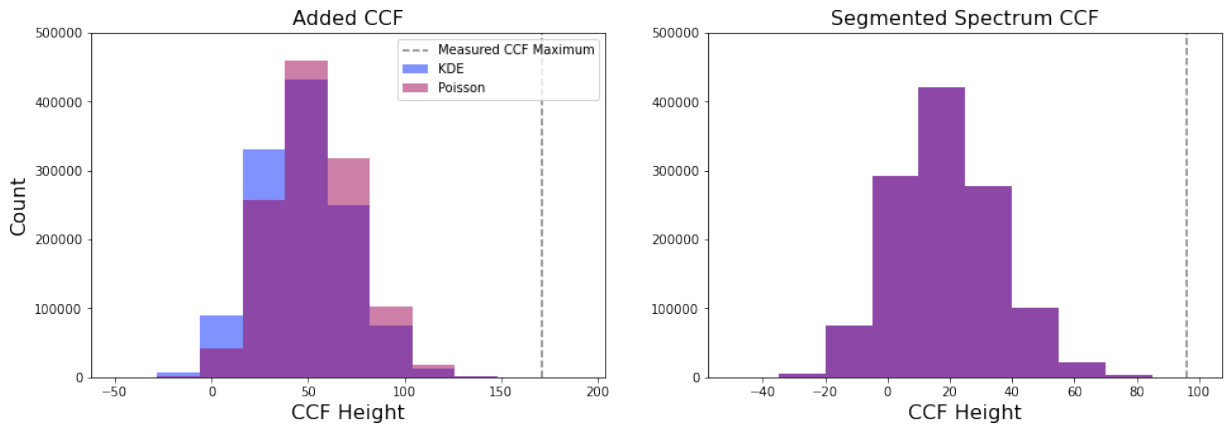


Figure 6. Distribution of CCF heights for simulations of noise cross-correlated with the [0,1] and [0,2] progressions of the H₂ template. Based on 1,200,000 simulations for each set, we detect H₂ at a level of 4.5σ for Poisson noise with the added CCFs, 4.6σ for KDE sampled noise with the added CCFs, 3.9σ for Poisson noise with the segmented spectrum CCF, and 4.0σ for KDE sampled noise with the segmented spectrum CCF.

range we used to look for a detection, as COS has a velocity precision of 15 km s^{-1} . This procedure was repeated multiple times (see Table 3) for each type of noise to produce the distributions shown in Figure 6. We then compared the CCF maximums to TWA 7’s CCF maximum within 15 km s^{-1} of the systemic velocity. The fraction of times the noise’s CCF maximum was equal to or larger than TWA 7’s CCF maximum is taken to be the probability of a false positive. The significance (σ) values we report are the equivalent probabilities for a Gaussian distribution.

We did an initial trial of 32,000 simulations with each method to see if we could detect each progression individually. We obtain significant detections for [0,1], [0,2], [1,4], and [1,7], with significant being defined as $>3\sigma$ detections for all four methods; we also get a marginal detection ($>3\sigma$ for some but not all methods) for [0,3] (Table 3). We then investigated the detected progressions further. Using a line strength cutoff of $5 \times 10^{-15} \text{ erg s}^{-1} \text{ cm}^{-2} \text{ \AA}^{-1}$, as shown in Figure 2, we detect H₂ at a significance $>5\sigma$ for all of our noise models and CCF types for the combination of the [1,4], [1,7], [0,1], and [0,2] progressions based on 3,500,000 simulations of each. For just the progressions on the wing — [0,1] combined with [0,2] — we did 1,200,000 simulations for each measurement. We detect H₂ at a level of 4.5σ for Poisson noise with the added CCFs, 4.6σ for KDE noise with the added CCFs, 3.9σ for Poisson noise with the segmented spectrum CCF, and 4.0σ for KDE sampled noise with the segmented spectrum CCF. The segmented

Table 3. Detection Significance of H₂ in Progressions

Progression	Added CCF		Segmented Spectrum CCF		Simulations	Minimum line strength erg s ⁻¹ cm ⁻² Å ⁻¹	Lines Included
	KDE	Poisson	KDE	Poisson			
[3, 13]	2.2	2.2	1.6	1.5	32000	0.1×10^{-15}	9
[4, 13]	0.7	0.7	0.8	0.8	32000	1.7×10^{-15}	2
[3, 16]	2.4	2.4	1.8	1.8	32000	1.2×10^{-15}	9
[4, 4]	1.2	1.2	2.0	2.0	32000	1.3×10^{-15}	6
[1, 7]	>4.0	>4.0	>4.0	>4.0	32000	7.5×10^{-15}	2
[1, 4]	>4.0	>4.0	>4.0	>4.0	32000	3.0×10^{-15}	12
[3, 0]	0.7	0.7	0.0	0.0	32000	3.5×10^{-15}	2
[0, 1]	3.5	3.4	3.2	3.1	32000	9.0×10^{-15}	2
[0, 2]	>4.0	>4.0	3.3	3.3	32000	5.0×10^{-15}	2
[2, 12]	2.2	2.3	2.6	2.6	32000	2.0×10^{-15}	2
[2, 15]	2.8	2.8	2.7	2.7	32000	3.0×10^{-15}	4
[0, 3]	3.3	3.1	2.9	2.8	32000	3.0×10^{-15}	5
[0, 1] + [0, 2]	4.6	4.5	4.0	3.9	1200000	5.0×10^{-15}	6
[1, 4] + [1, 7] + [0, 1] + [0, 2]	>5.0	>5.0	>5.0	>5.0	3500000	5.0×10^{-15}	20

NOTE—Significance of detection in each individual progression for our four different methods, as well as for the combination of [0,1] and [0,2] and the combination of [1,4], [1,7], [0,1], and [0,2].

spectrum CCF produces similar distributions for both types of noise, as shown on the right of Figure 6, because it is more robust to slight differences in noise models.

There are two unclassified background objects in the sky near TWA 7. However, the two sources are not expected to be in the COS-PSA aperture, given the COS-PSA aperture size of 2.5" in diameter and the distance of the background sources to TWA 7, at 2.5" (Neuhäuser et al. 2000) and 6" (Bayo et al. 2019), given we confirmed that TWA 7 was centered on the aperture. Furthermore, as we required that the CCF peak at the radial velocity of the object fall within the error of the spectrograph, we feel these background sources are an extremely unlikely source of the H₂.

3.3. Determining the Origin of the H₂

Simply detecting H₂ does not indicate that the H₂ is circumstellar in origin, because some M stars are known to show H₂ emission pumped by Ly α (Kruczek et al. 2017). Active M stars, like TWA 7 (Yang et al. 2008), have strong chromospheric Ly α emission, which can pump H₂ in star spots or in their lower chromospheres. Since TWA 7's debris disk is nearly face on at an inclination of 13° (Olofsson et al. 2018), and the resolution of COS is 15 km/s, we cannot use velocity information to differentiate between circumstellar and stellar H₂. Instead, we looked at the flux ratios between different progressions. The [1,4] and [1,7] progression are both pumped by emission from the center of the Ly α line profile (Figure 3). Other progressions are pumped from the wings of the profile, so strong emission in these lines is only possible with a broader Ly α line indicative of active accretion. The two most prominent examples are [0,1] and [0,2] which are pumped at velocities 379 and 487 km/s from line center. These progressions should only be bright if the Ly α profile is especially wide, as shown in the purple profile in Figure 3, but they will be much fainter if the star's Ly α profile is more narrow, similar to the pink curve. Stars that are accreting have much broader Ly α profiles than active main sequence stars (Schindhelm et al. 2012; Youngblood et al. 2016) and are therefore expected to produce more emission in the [0,1] and [0,2] progressions relative to the [1,4] and [1,7] progressions in comparison to non-accretors.

Using the segmented spectrum, we took the ratio of the CCF maximum of all the non-central progressions to the ratio of the CCF maximum of [1,4]+[1,7] for all the stars with previously detected H₂ in our sample. Dividing by the height of [1,4]+[1,7] for each system acts as a normalization factor to deal with spectra with different S/N or different line widths due to rotational broadening. Since this ratio can be affected by extinction, with lines at shorter wavelengths appearing fainter than they are intrinsically, we have to de-redden the spectrum first, which we do based

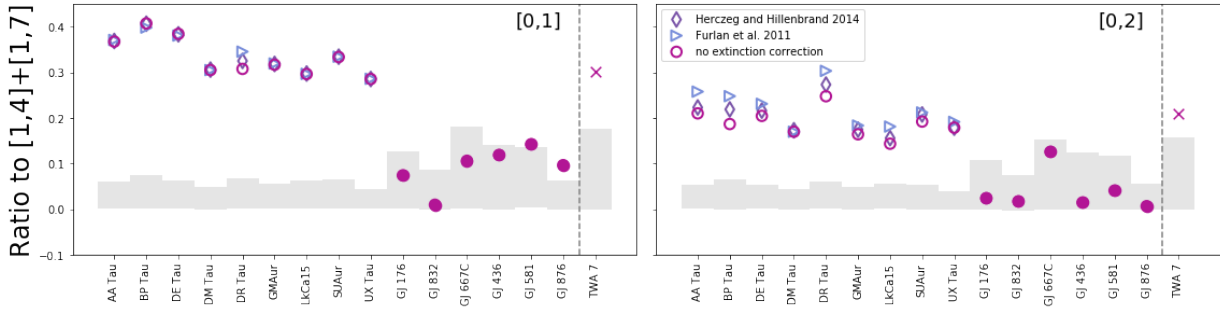


Figure 7. The CCF height ratios of [0,1] and [0,2] to that of [1,4]+[1,7] for our selection of T Tauri stars (open symbols), M stars (filled symbols), and TWA 7. The gray areas are the 1σ regions for a null result if that progression had no flux and just noise. They are greater than zero because we select the maximum of the CCF within 15 km s^{-1} , which would typically be greater than zero even for random noise. TWA 7’s ratios matches better with the T Tauri stars, suggesting that its H_2 is also circumstellar. The ratios for the other progressions are shown in the appendix in Figure A1.

on the extinction laws from Cardelli et al. (1989). We examine three different sets of ratios: ratios with spectra uncorrected for extinction, ratios with spectra corrected by the extinction values found by Furlan et al. (2011), and ratios with spectra corrected by extinction values from Herczeg & Hillenbrand (2014). We assume the main sequence M stars and TWA 7 have no extinction based on extinction measurements from stars in the Local Bubble (Leroy 1993).

To estimate the 1σ limits (the gray areas in Figures 7 and A1), we used a similar procedure as we used to calculate the significance of detections for TWA 7. We sampled the noise from each spectrum, calculating a KDE like we did for TWA 7, and created spectra of pure noise to cross-correlate with the template. We then took the maximum of each CCF within 15 km/s of the RV of that star. The gray regions represent the inner 68% of ratios calculated based on those maxima. These 1σ regions are biased towards positive numbers, because we chose the maximum CCF value, which even in a normally distributed, random noise sample will bias to positive values.

The [0,1] and [0,2] ratios differentiate the samples most clearly regardless of extinction correction. Based on their data, TWA 7’s H_2 appears to be more similar to that from the CTTS (Figure 7). However, other progressions are not as clear. To analyze all of the ratios, we created a Support Vector Machine classifier (Platt 1999) with a 4th order polynomial kernel using the data from the M dwarfs and CTTS — excluding TWA 7 — to determine where the H_2 was coming from. We then applied this classification scheme to the TWA 7 data. Based on the observed ratios, this test categorizes TWA 7’s H_2 as similar to CTTS’ 99.2% of the time for the set uncorrected for extinction, 98.2% of the time for the set corrected using the extinction values from Herczeg & Hillenbrand (2014), and 98.3% of the time for the set corrected using the extinction values from Furlan et al. (2011). This implies that the TWA 7’s H_2 is being pumped not only from the core, but also from the wings of the $\text{Ly}\alpha$ profile as with CTTS. We expand upon this in Section 4.

3.4. Estimating the Amount of Circumstellar H_2

To estimate the amount of warm H_2 in TWA 7, we compared its H_2 emission with that of a transition disk system, TW Hya. We chose TW Hya because in comparison with TWA 7, it has a similar age (Webb et al. 1999), inclination (Pontoppidan et al. 2008), and a relatively similar spectral type (Herczeg & Hillenbrand 2014). While we do not think that the line profile of TW Hya would be identical to that of TWA 7, as TW Hya is accreting enough to be measured by conventional methods, it is the best match from the data available. Our goal was to find a constant scale factor that is the ratio between the H_2 line strengths in TWA 7 and those in TW Hya. We used a least squares fit to calculate this scale factor with the only other free parameter being the radial velocity difference. We coadded the 19 brightest H_2 features from the most prominent progressions — [1,4], [1,7], [0,1], and [0,2] — and compared the line flux from the coadded profile to the coadded profile from TW Hya. We also measured the uncertainty of this ratio by measuring the noise in the spectrum in comparison to the flux. We found a ratio between the coadded profiles of $(6.9 \pm 0.7) \times 10^{-4}$. as shown in Figure 8. Adjusting for differences in distance, TWA 7 has $(2.2 \pm 0.2) \times 10^{-4}$ of TW Hya’s H_2 line strength, and, as a result of its similar inclination and line widths, its H_2 luminosity is assumed to be less than TW Hya’s by the same factor. France et al. (2012) measure TW Hya’s H_2 luminosity as $(16.2 \pm 2.0) \times 10^{29} \text{ erg s}^{-1}$. This gives us an H_2 luminosity of $(3.6 \pm 0.6) \times 10^{26} \text{ erg s}^{-1}$ for TWA 7. By comparing the flux values measured by Kruczek et al. (2017)

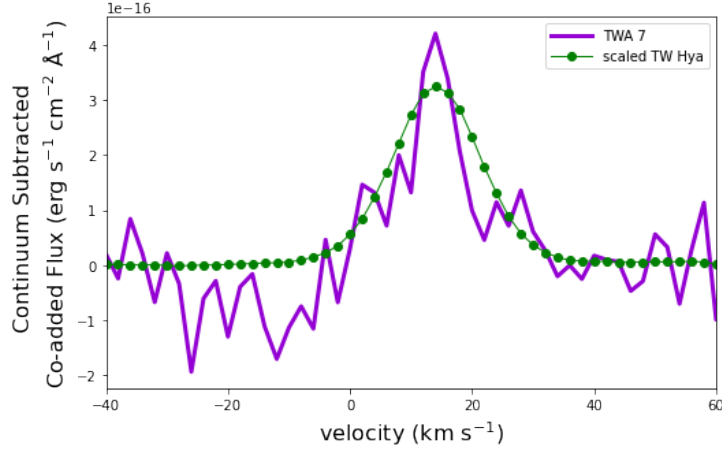


Figure 8. The co-added H₂ line profile of TWA 7 compared to the co-added line profile of TW Hya, scaled by the best fit ratio of $(6.9 \pm 0.7) \times 10^{-4}$.

in star spots to our value for TWA 7’s flux, even if there is a contribution from star spots to this value, we expect that the circumstellar gas is more than 50% of the total H₂ luminosity.

From this scaling factor, we can also put a lower limit on the mass of warm H₂ assuming the gas is all circumstellar. The flux observed in a specific H₂ line, F_{obs} , is a function of the Einstein A value for that emitting transition, A_{Bl} , the distance to TWA 7, d , the frequency of the emitting transition, ν_{Bl} , and the number of H₂ molecules that have been pumped to the required electronic excited state, N_B :

$$F_{obs} = N_B \frac{A_{Bl} h \nu_{Bl}}{4\pi d^2} \quad (1)$$

where l is a lower energy state than B .

N_B depends on the number of H₂ molecules in the lower state of the pumping transition, N_X and the rate at which those get excited. This rate is dependent on the oscillator strength f , the Ly α flux of TWA 7, and the optical depth of the warm H₂. Since we do not know the Ly α flux, the H₂ filling factor, or the optical depth, we instead choose to estimate an upper limit for the excitation rate, which turns into a lower limit for N_X as described by Equation 2:

$$N_X \frac{4\pi J_\nu}{h\nu_p} \frac{\pi e^2}{m_e c} f \leq N_B \sum A_{Bl} \quad (2)$$

where A_{Bl} are all the relevant Einstein A values for the upper state, J_ν is the Ly α flux at the pumping wavelength, and ν_p is the frequency of the pumping transition. We do not consider dissociation, as the probability of dissociation for [1,4], [1,7], [0,1], and [0,2] is predicted to be negligible (Abgrall et al. 2000). This N_X is dependent on the total number of warm H₂ molecules, N_{H_2} , and the temperature, which gets factored into the Boltzmann Equation, $q(T)$:

$$q(T)N_{H_2} = N_X. \quad (3)$$

We calculate a $q(T)$ based on the assumption that the H₂ is being thermally excited (Ádámkóvics et al. 2016).

While Ly α flux varies in time, and the HST FUV observation of TWA 7’s Ly α flux is contaminated by ISM absorption and geocoronal emission, we estimate that TWA 7’s Ly α is less than 0.03 of TW Hya’s based on comparison of the spectra at velocities >400 km/s (Herczeg et al. 2004). We estimate the flux observed for a given transition using our scaling factor found above and the flux observed for TW Hya by Herczeg et al. (2002). All pumping transition properties are described in Table 2, while the Einstein A values are from (Abgrall et al. 1993). We calculate a separate N_{H_2} for each line flux measured for TW Hya, which then converts into a line flux for TWA 7; we then average these values together to get our final result. For a gas temperature of 1500 K, we get a rough estimate for the minimum amount of warm H₂ of $\sim 9.9 \times 10^{-11} M_\oplus$. If spread out in a ring with a radius of 0.3 AU — a radius at which H₂ is commonly seen (France et al. 2012) — this corresponds to a minimum column density of $\sim 2.8 \times 10^{15} \text{ cm}^{-2}$. This is consistent with the upper limit on H₂ column density reported by Ingleby et al. (2009) of $3.0 \times 10^{17} \text{ cm}^{-2}$ using a less

sensitive prism spectrum of TWA 7. Based on the spread of line fluxes, we adopt a range of 10^{15} to 3.0×10^{17} cm^{-2} for the vertical column density of H_2 in TWA 7.

4. DISCUSSION

The H_2 progressions ratios from TWA 7 (Figure 7) more closely resemble that from CTTS than that from M stars. However, these ratios do not guarantee that the H_2 is circumstellar. TWA 7 is much closer in age to the CTTS and is thus likely to have higher chromospheric activity than an average M star. Chromospheric activity produces $\text{Ly}\alpha$ emission, which can then excite the H_2 in star spots on mid M type stars. We suggest this is not the primary source of H_2 emission in TWA 7 as chromospheric activity affects the core of the $\text{Ly}\alpha$ profile significantly more than the wings (Lemaire et al. 2015). So while there is some $\text{Ly}\alpha$ emission in the wings from all of these stars, the amount of flux induced solely from chromospheric activity is likely not enough to excite the outer H_2 progressions. Youngblood et al. (2021) looked at how $\text{Ly}\alpha$ varied with stellar parameters, showing how increased $\text{Ly}\alpha$ is correlated with higher chromospheric activity and lower gravity, both of which are correlated with youth. However, the profiles from Youngblood et al. (2021) show that the ratio of the flux between the peak and the wings can remain constant with varying chromospheric activity and gravity, even if the overall flux changes. Thus the most likely explanation is that TWA 7 is still weakly accreting circumstellar gas from an inner disk.

Accretion rates for weakly accreting stars are notoriously hard to measure accurately. There are cases, like MY Lup, that have FUV accretion signatures but lack optical ones (Alcalá et al. 2019). Previously, TWA 7 was considered a standard, non-accreting WTTS. It shows no accretion signatures in the optical. The hot FUV lines seen in TWA 7's HST-COS spectrum, such as C IV or N V, have profiles that do not look like those of CTTS (Ardila et al. 2013). It also lacks the NUV flux and Ca II] $\lambda 2325$ emission of known accreting stars (Ingleby et al. 2011b, 2013). However, most of the accreting gas is expected to be hydrogen in the ground state (Muzerolle et al. 2000), so $\text{Ly}\alpha$ should be more sensitive to small accretion rates than any other line. There is a similar system in TWA, TWA 4 B, a K5 star with circumstellar H_2 FUV emission discovered by Yang et al. (2012) despite not showing obvious accretion signatures. Given TWA is close in age to when the typical protoplanetary disk is predicted to evolve into a debris disk, these systems could represent a short-lived phase of disk evolution with residual gas that does not accrete at the high levels detectable in optical spectra. FUV spectra of more stars in TWA would allow us to further investigate the gas evolution at this crucial age.

Assuming the H_2 we observe is indeed circumstellar, the next question concerns its origin. One possibility is that the H_2 originates from the inward migration, sublimation, and the subsequent photodissociation of H_2O ices in comet-like nuclei. The H_2O photodissociates into H, OH, and O, and the newly available H atoms can then reform into H_2 . If true, there should also be some oxygen gas species in the inner disk. Riviere-Marichalar et al. (2013) give an upper limit on the oxygen mass of $2.3 \times 10^{-5} M_{\oplus}$ from Herschel data. This upper limit is more than the oxygen that would accompany the H_2 we detect if the H_2 originates from dissociated H_2O and assuming the warm H_2 is confined to the inner few AU of the disk, making this a potentially viable source of the observed H_2 . Future observations could better constrain the oxygen mass in the inner disk and allow us to determine whether H_2O ice evaporation is a possible origin of the circumstellar H_2 around TWA 7. Additionally, detection of dust from these comets could lend support to this theory (Pearce et al. 2020).

Another possibility is that the H_2 we see is residual protoplanetary disk gas. Regardless of its origin, an H_2 formation pathway is needed to balance ongoing UV photodissociation of H_2 . Molecular hydrogen forms most efficiently on grain surfaces, as in the ISM, but it can also form via gas phase reactions (e.g., through $\text{H} + \text{H}^- \rightarrow \text{H}_2 + \text{e}^-$) when there is less dust surface area available (Bruderer 2013).

To explore the possibility of grain surface formation of H_2 in the case of TWA 7, we can estimate the upper limit on the surface area of warm grains by looking at its spectral energy distribution (SED). Although the W3 band from WISE (Wright et al. 2010) shows no excess IR emission from dust (Olofsson et al. 2018; Bayo et al. 2019), we can put a limit on the amount of warm dust by assuming the dust can generate the equivalent of the 1σ uncertainty for the W3 flux. Under that assumption, we compute the SED using the model described by Isella & Natta (2005) to put an upper limit of $\leq 5.1 \times 10^{-8} M_{\oplus}$ on the amount of warm (~ 1000 K) silicate particles between $1 \mu\text{m}$ and 1mm . We chose a lower particle size limit of $1 \mu\text{m}$, because in more evolved systems, particles smaller than that near the star can get blown away by stellar winds. Based on this estimate, grains with radii between $1 \mu\text{m}$ and 1mm could make up a significant surface area, up to a surface area of 10^{23}cm^2 . If the grains are spread out evenly over the inner 0.3 au, the mass column density is $2 \times 10^{-5} \text{g cm}^{-2}$.

With the above constraint on the possible dust content of the inner disk of TWA 7, we can use the results of [Bruderer \(2013\)](#) to estimate the H₂ reservoir that can be sustained in the inner disk. In modeling the inner regions of transition disks, [Bruderer \(2013\)](#) considered two physical models: a dusty inner disk and a very dust-poor inner disk with dust column densities of $\Sigma_d=3\times 10^{-4}$ g cm⁻² and 3×10^{-9} g cm⁻² respectively at 0.3 au. The upper limit on the dust surface density of TWA 7 we find above is an order of magnitude below the surface density of the dusty inner disk model but many orders of magnitude above the surface density of the dust-poor disk model. Thus the dust-poor disk model provides a relatively conservative estimate of the H₂ density allowed for TWA 7.

The other relevant parameter in the [Bruderer \(2013\)](#) model is the gas surface density. Figure 6 of [Bruderer \(2013\)](#) shows the results for a case in which the inner disk is very dust poor and has a gas column density of 0.3 g cm⁻² at 0.3 au. The H₂ fraction in the disk atmosphere is $\sim 3\times 10^{-6}$ relative to hydrogen or an H₂ column density of $N_{\text{H}_2}=3\times 10^{18}$ g cm⁻². [Bruderer \(2013\)](#) do not show the temperature of the H₂, although much of it is likely to be warm, as the disk is dust poor, and dust is a coolant for the gas through gas-grain collisions. If 0.1% of the total H₂ column is warm (~ 1500 K), this scenario predicts a warm H₂ mass similar to that inferred for TWA 7.

Note that this result is obtained despite using a model with a dust density several orders of magnitude below our dust upper limit. Thus, it seems plausible that even a dust-poor inner disk can sustain a warm H₂ column density in the range we estimate for TWA 7 in Section 3.4. While the models from [Bruderer \(2013\)](#) were not tuned specifically to TWA 7's parameters — the model assumes a hotter 10 L_⊙ star and a given polycyclic aromatic hydrocarbons (PAH) abundance — these two factors should impact the H₂ production in opposite ways: the higher UV flux of the more massive star enhances photodestruction of H₂, while the PAH abundance enhances H₂ production. We therefore believe it is plausible that the H₂ we detect is sustained via some combination of gas phase reactions in the circumstellar environment of TWA 7. Future observations between 3 and 12 microns with telescopes like JWST could detect PAHs in the disk and lend further support to this possibility ([Seok & Li 2017](#)).

Although we do not have the requisite measurements to conclusively determine why there is warm H₂ in the circumstellar environment of TWA 7, regardless of its origin, warm gas in a region without detectable warm dust is not unique to this star. Primordial warm H₂ is detected inside the inner edge of the dust disk in transitional disk systems ([France et al. 2012](#); [Arulanantham et al. 2018](#)). Warm CO has also been detected in these regions ([Pontoppidan et al. 2008](#); [Salyk et al. 2011](#)). Clearly, warm gas can outlast detectable amounts of warm dust. Thus, the physics resulting in warm gas in the cavities of transitional disks could also be the cause of the H₂ we detect in TWA 7.

5. CONCLUSIONS

We have detected molecular hydrogen from four progressions ([1,4], [1,7], [0,1], and [0,2]) in TWA 7, a known debris disk system. The ratios between CCF peaks of the detected H₂ progressions (Figure 7) resemble those from CTTS. This suggests that the H₂ in TWA 7 is circumstellar, as it is for CTTS. This is highly unexpected, because H₂ is not typically detected in debris disk systems. This star joins a small group of systems that have H₂ but are not accreting by typical diagnostic standards. Assuming the H₂ is circumstellar, we have estimated a column density of 10¹⁵ to 3.0×10¹⁷ cm⁻². While we cannot determine the origin of the gas conclusively, it is likely to be generated from residual protoplanetary disk gas.

ACKNOWLEDGMENTS

Based on observations with the NASA/ESA Hubble Space Telescope obtained at the Space Telescope Science Institute, which is operated by the Association of Universities for Research in Astronomy, Incorporated, under NASA contract NAS5-26555. Support for program number (GO-15310) was provided through a grant from the STScI under NASA contract NAS5-26555. G.J.H. is supported by general grant 11773002 awarded by the National Science Foundation of China. L.F. would like to thank Andrea Isella for help with the S.E.D. modeling. This research has made use of the VizieR catalogue access tool, CDS, Strasbourg, France. The original description of the VizieR service was published by ([Wenger et al. 2000](#)). This research has made use of the SIMBAD database, operated at CDS, Strasbourg, France. This research has made use of the NASA/ IPAC Infrared Science Archive, which is operated by the Jet Propulsion Laboratory, California Institute of Technology, under contract with the National Aeronautics and Space Administration. This work has made use of data from the European Space Agency (ESA) mission *Gaia* (<https://www.cosmos.esa.int/gaia>), processed by the *Gaia* Data Processing and Analysis Consortium (DPAC, <https://www.cosmos.esa.int/web/gaia/dpac/consortium>). Funding for the DPAC has been provided by national institutions, in particular the institutions participating in the *Gaia* Multilateral Agreement.

Facility: HST (COS, STIS)

Software: SpecTres (Carnall 2017), NumPy (Oliphant 2006; Van Der Walt et al. 2011), Scikit-learn (Pedregosa et al. 2011), Pandas (pandas development team 2020), Scipy (Virtanen et al. 2019), Matplotlib (Hunter 2007)

APPENDIX

A. CCF RATIOS

We took the ratio of the CCF maximum of all the non-central progressions to the ratio of the CCF maximum of [1,4]+[1,7] for all the stars with previously detected H₂ in our sample. In Figure A1, we plot all of these ratios. TWA 7's ratios were statistically more similar to that of the CTTS than that of the main sequence M dwarfs. We describe this analysis in detail in Section 3.3.

[0,1] and [0,2] have the most easily detectable flux because of a combination of several factors regarding the pumping transition shown in Table 2: relatively close to the center of Ly α , high oscillators strengths, and low energy levels for the lower state of the ground pumping transition.

REFERENCES

- Abgrall, H., Roueff, E., & Drira, I. 2000, *Astronomy and Astrophysics Supplement Series*, 141, 297.
<http://adsabs.harvard.edu/abs/2000A%26AS..141..297A>
- Abgrall, H., Roueff, E., Launay, F., Roncin, J. Y., & Subtil, J. L. 1993, *Astronomy and Astrophysics Supplement Series*, 101, 273.
<http://adsabs.harvard.edu/abs/1993A%26AS..101..273A>
- Ádámkóvics, M., Najita, J. R., & Glassgold, A. E. 2016, *The Astrophysical Journal*, 817, 82.
<http://adsabs.harvard.edu/abs/2016ApJ...817...82A>
- Aikawa, Y., Furuya, K., Hincelin, U., & Herbst, E. 2018, *The Astrophysical Journal*, 855, 119.
<http://adsabs.harvard.edu/abs/2018ApJ...855..119A>
- Alcalá, J. M., Manara, C. F., France, K., et al. 2019, *Astronomy and Astrophysics*, 629, A108.
<https://ui.adsabs.harvard.edu/abs/2019A%26A...629A.108A/abstract>
- Andrews, S. M., Huang, J., Pérez, L. M., et al. 2018, *The Astrophysical Journal*, 869, L41. <https://ui.adsabs.harvard.edu/abs/2018ApJ...869L..41A/abstract>
- Ardila, D. R., Basri, G., Walter, F. M., Valenti, J. A., & Johns-Krull, C. M. 2002, *The Astrophysical Journal*, 566, 1100. <http://stacks.iop.org/0004-637X/566/i=2/a=1100>
- Ardila, D. R., Herczeg, G. J., Gregory, S. G., et al. 2013, *The Astrophysical Journal Supplement Series*, 207, 1.
<https://ui.adsabs.harvard.edu/abs/2013ApJS..207....1A/abstract>
- Arulanantham, N., France, K., Hoadley, K., et al. 2018, *The Astrophysical Journal*, 855, 98.
<http://adsabs.harvard.edu/abs/2018ApJ...855...98A>
- Ayres, T. R. 2015, *The Astronomical Journal*, 149, 58.
<https://ui.adsabs.harvard.edu/abs/2015AJ....149...58A/abstract>
- Bailer-Jones, C. a. L., Rybizki, J., Foesneau, M., Mantelet, G., & Andrae, R. 2018, *The Astronomical Journal*, 156, 58.
<https://ui.adsabs.harvard.edu/#abs/arXiv:1804.10121>
- Baruteau, C., Crida, A., Paardekooper, S.-J., et al. 2014, *Protostars and Planets VI*, 667.
<http://adsabs.harvard.edu/abs/2014prpl.conf..667B>
- Bary, J. S., Weintraub, D. A., & Kastner, J. H. 2003, *The Astrophysical Journal*, 586, 1136.
<http://adsabs.harvard.edu/abs/2003ApJ...586.1136B>
- Bayo, A., Olofsson, J., Matrà, L., et al. 2019, *Monthly Notices of the Royal Astronomical Society*, 486, 5552.
<https://ui.adsabs.harvard.edu/abs/2019MNRAS.486.5552B/abstract>
- Bitner, M. A., Richter, M. J., Lacy, J. H., et al. 2008, *The Astrophysical Journal*, 688, 1326. <https://ui.adsabs.harvard.edu/abs/2008ApJ...688.1326B/abstract>
- Brandt, J. C., Heap, S. R., Walter, F. M., et al. 2001, *The Astronomical Journal*, 121, 2173. <https://ui.adsabs.harvard.edu/abs/2001AJ....121.2173B/abstract>
- Bruderer, S. 2013, *Astronomy and Astrophysics*, 559, A46.
<https://ui.adsabs.harvard.edu/abs/2013A%26A...559A..46B/abstract>
- Cardelli, J. A., Clayton, G. C., & Mathis, J. S. 1989, *The Astrophysical Journal*, 345, 245. <https://ui.adsabs.harvard.edu/abs/1989ApJ...345..245C/abstract>
- Carmona, A., van den Ancker, M. E., Henning, T., et al. 2008, *Astronomy and Astrophysics*, 477, 839.
<http://adsabs.harvard.edu/abs/2008A%26A...477..839C>

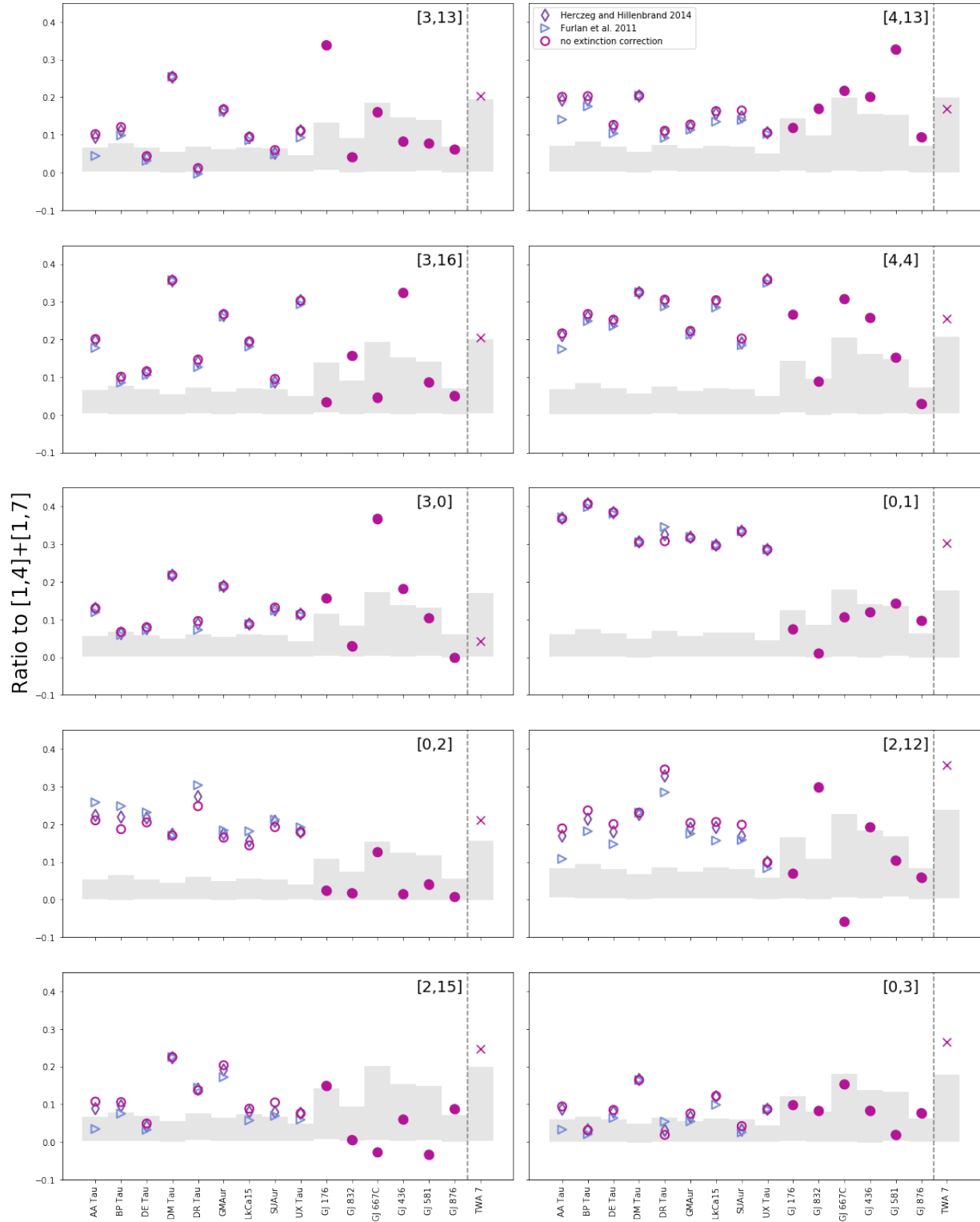


Figure A1. The CCF height ratios of non-central progressions to that of [1,4]+[1,7] for our selection of T Tauri stars (open symbols), M stars (filled symbols), and TWA 7. The gray areas are the 1σ regions for a null result if that progression had no flux and just noise. They are greater than zero because we select the maximum of the CCF within 15 km s^{-1} , which would typically be greater than zero even for random noise. TWA 7's ratios matches better with the T Tauri stars, suggesting that its H₂ is also circumstellar.

- Carnall, A. C. 2017, arXiv:1705.05165 [astro-ph].
<https://arxiv.org/abs/1705.05165>
- Chen, C. H., Li, A., Bohac, C., et al. 2007, *The Astrophysical Journal*, 666, 466. <https://ui.adsabs.harvard.edu/abs/2007ApJ...666..466C/abstract>
- Choquet, É., Perrin, M. D., Chen, C. H., et al. 2016, *The Astrophysical Journal*, 817, L2.
<https://arxiv.org/abs/1512.02220>
- Cieza, L. A., Olofsson, J., Harvey, P. M., et al. 2013, *The Astrophysical Journal*, 762, 100. <https://ui.adsabs.harvard.edu/abs/2013ApJ...762..100C/abstract>
- Collaboration, G., Brown, A. G. A., Vallenari, A., et al. 2018, *Astronomy and Astrophysics*, 616, A1.
<https://ui.adsabs.harvard.edu/abs/2018A%26A...616A...1G/abstract>
- Danforth, C. W., Keeney, B. A., Stocke, J. T., Shull, J. M., & Yao, Y. 2016, *The Astrophysical Journal*, 828, 69.
<https://ui.adsabs.harvard.edu/abs/2016ApJ...828...69M/abstract>
- Dashtamirova, D., Fischer, W. J., et al. 2020, STSci, Baltimore
- Dent, W. R. F., Wyatt, M. C., Roberge, A., et al. 2014, *Science*, 343, 1490.
<http://adsabs.harvard.edu/abs/2014Sci...343.1490D>
- Favre, C., Cleeves, L. I., Bergin, E. A., Qi, C., & Blake, G. A. 2013, *The Astrophysical Journal Letters*, 776, L38.
<http://adsabs.harvard.edu/abs/2013ApJ...776L..38F>
- France, K., Herczeg, G. J., McJunkin, M., & Penton, S. V. 2014, *The Astrophysical Journal*, 794, 160.
<http://adsabs.harvard.edu/abs/2014ApJ...794..160F>
- France, K., Roberge, A., Lupu, R. E., Redfield, S., & Feldman, P. D. 2007, *The Astrophysical Journal*, 668, 1174.
<http://adsabs.harvard.edu/abs/2007ApJ...668.1174F>
- France, K., Roueff, E., & Abgrall, H. 2017, *The Astrophysical Journal*, 844, 169.
<http://adsabs.harvard.edu/abs/2017ApJ...844..169F>
- France, K., Schindhelm, E., Herczeg, G. J., et al. 2012, *The Astrophysical Journal*, 756, 171.
<http://adsabs.harvard.edu/abs/2012ApJ...756..171F>
- Furlan, E., Luhman, K. L., Espaillat, C., et al. 2011, *The Astrophysical Journal Supplement Series*, 195, 3.
<https://ui.adsabs.harvard.edu/abs/2011ApJS..195....3F/abstract>
- Goldreich, P., & Sari, R. 2003, *The Astrophysical Journal*, 585, 1024.
<http://adsabs.harvard.edu/abs/2003ApJ...585.1024G>
- Gonzalez, J.-F., Laibe, G., & Maddison, S. T. 2017, *Monthly Notices of the Royal Astronomical Society*, 467, 1984.
<http://adsabs.harvard.edu/abs/2017MNRAS.467.1984G>
- Hartmann, L., & Kenyon, S. J. 1987, *The Astrophysical Journal*, 312, 243.
<http://adsabs.harvard.edu/abs/1987ApJ...312..243H>
- Herczeg, G. J., & Hillenbrand, L. A. 2014, *The Astrophysical Journal*, 786, 97.
<http://adsabs.harvard.edu/abs/2014ApJ...786...97H>
- Herczeg, G. J., Linsky, J. L., Valenti, J. A., Johns-Krull, C. M., & Wood, B. E. 2002, *The Astrophysical Journal*, 572, 310. <https://ui.adsabs.harvard.edu/abs/2002ApJ...572..310H/abstract>
- Herczeg, G. J., Linsky, J. L., Walter, F. M., Gahm, G. F., & Johns-Krull, C. M. 2006, *The Astrophysical Journal Supplement Series*, 165, 256.
<http://adsabs.harvard.edu/abs/2006ApJS..165..256H>
- Herczeg, G. J., Wood, B. E., Linsky, J. L., Valenti, J. A., & Johns-Krull, C. M. 2004, *The Astrophysical Journal*, 607, 369.
<http://adsabs.harvard.edu/abs/2004ApJ...607..369H>
- Higuchi, A. E., Sato, A., Tsukagoshi, T., et al. 2017, *The Astrophysical Journal Letters*, 839, L14.
<http://adsabs.harvard.edu/abs/2017ApJ...839L..14H>
- Hunter, J. D. 2007, *Computing in Science & Engineering*, 9, 90
- Ingleby, L., Calvet, N., Hernández, J., et al. 2011a, *The Astronomical Journal*, 141, 127. <https://ui.adsabs.harvard.edu/abs/2011AJ...141..127I/abstract>
- Ingleby, L., Calvet, N., Bergin, E., et al. 2009, *The Astrophysical Journal Letters*, 703, L137.
<http://adsabs.harvard.edu/abs/2009ApJ...703L.137I>
- . 2011b, *The Astrophysical Journal*, 743, 105. <https://ui.adsabs.harvard.edu/abs/2011ApJ...743..105I/abstract>
- Ingleby, L., Calvet, N., Herczeg, G., et al. 2013, *The Astrophysical Journal*, 767, 112.
<https://ui.adsabs.harvard.edu/#abs/arXiv:1303.0769>
- Isella, A., & Natta, A. 2005, *A&A*, 438, 899.
<http://www.aanda.org/10.1051/0004-6361:20052773>
- Jayawardhana, R., Coffey, J., Scholz, A., Brandeker, A., & van Kerkwijk, M. H. 2006, *The Astrophysical Journal*, 648, 1206. <https://ui.adsabs.harvard.edu/abs/2006ApJ...648.1206J/abstract>
- Jensen, E. L. N., Cohen, D. H., & Gagné, M. 2009, *The Astrophysical Journal*, 703, 252.
<http://adsabs.harvard.edu/abs/2009ApJ...703..252J>
- Kenyon, S. J., & Bromley, B. C. 2006, *The Astronomical Journal*, 131, 1837.
<http://adsabs.harvard.edu/abs/2006AJ...131.1837K>

- Kenyon, S. J., Najita, J. R., & Bromley, B. C. 2016, *The Astrophysical Journal*, 831, 8. <https://ui.adsabs.harvard.edu/abs/2016ApJ...831....8K/abstract>
- Kruczek, N., France, K., Evonosky, W., et al. 2017, *The Astrophysical Journal*, 845, 3. <http://adsabs.harvard.edu/abs/2017ApJ...845....3K>
- Lemaire, P., Vial, J.-C., Curdt, W., Schühle, U., & Wilhelm, K. 2015, *Astronomy and Astrophysics*, 581, A26. <https://ui.adsabs.harvard.edu/abs/2015A%26A...581A..26L/abstract>
- Leroy, J. L. 1993, *Astronomy and Astrophysics*, 274, 203. <http://adsabs.harvard.edu/abs/1993A%26A...274..203L>
- Lestrade, J.-F., Matthews, B. C., Sibthorpe, B., et al. 2012, *Astronomy and Astrophysics*, 548, A86. <https://ui.adsabs.harvard.edu/abs/2012A%26A...548A..86L/abstract>
- Linsky, J. L., Bushinsky, R., Ayres, T., & France, K. 2012, *The Astrophysical Journal*, 754, 69. <https://ui.adsabs.harvard.edu/abs/2012ApJ...754...69L/abstract>
- Low, F. J., Smith, P. S., Werner, M., et al. 2005, *The Astrophysical Journal*, 631, 1170. <https://ui.adsabs.harvard.edu/abs/2005ApJ...631.1170L/abstract>
- Loyd, R. O. P., France, K., Youngblood, A., et al. 2016, *The Astrophysical Journal*, 824, 102. <http://adsabs.harvard.edu/abs/2016ApJ...824..102L>
- Lyra, W., & Kuchner, M. 2013, *Nature*, 499, 184. <http://adsabs.harvard.edu/abs/2013Natur.499..184L>
- Manara, C. F., Testi, L., Rigliaco, E., et al. 2013, *Astronomy and Astrophysics*, 551, A107. <http://adsabs.harvard.edu/abs/2013A%26A...551A.107M>
- Matrà, L., Öberg, K. I., Wilner, D. J., Olofsson, J., & Bayo, A. 2019, *The Astronomical Journal*, 157, 117. <http://stacks.iop.org/1538-3881/157/i=3/a=117?key=crossref.7d97b74a8132d50624fc655e1a15f805>
- Matthews, B. C., Kalas, P. G., & Wyatt, M. C. 2007, *The Astrophysical Journal*, 663, 1103. <http://stacks.iop.org/0004-637X/663/i=2/a=1103>
- Matthews, B. C., Krivov, A. V., Wyatt, M. C., Bryden, G., & Eiroa, C. 2014, *Protostars and Planets VI*, 521. <https://ui.adsabs.harvard.edu/abs/2014prpl.conf..521M/abstract>
- McClure, M. K. 2019, *Astronomy and Astrophysics*, 632, A32. <http://adsabs.harvard.edu/abs/2019A%26A...632A..32M>
- McJunkin, M., France, K., Schindhelm, E., et al. 2016, *The Astrophysical Journal*, 828, 69. <https://ui.adsabs.harvard.edu/abs/2016ApJ...828...69M/abstract>
- Molyarova, T., Akimkin, V., Semenov, D., et al. 2017, *The Astrophysical Journal*, 849, 130. <http://adsabs.harvard.edu/abs/2017ApJ...849..130M>
- Moór, A., Ábrahám, P., Juhász, A., et al. 2011, *The Astrophysical Journal Letters*, 740, L7. <http://adsabs.harvard.edu/abs/2011ApJ...740L...7M>
- Mumma, M. J., & Charnley, S. B. 2011, *Annual Review of Astronomy and Astrophysics*, 49, 471. <https://ui.adsabs.harvard.edu/2011ARA&A..49..471M/abstract>
- Muzerolle, J., Briceño, C., Calvet, N., et al. 2000, *The Astrophysical Journal Letters*, 545, L141. <http://adsabs.harvard.edu/abs/2000ApJ...545L.141M>
- Neuhäuser, R., Brandner, W., Eckart, A., et al. 2000, *Astronomy and Astrophysics*, 354, L9. <https://ui.adsabs.harvard.edu/abs/2000A%26A...354L...9N/abstract>
- Nguyen, D. C., Brandeker, A., van Kerkwijk, M. H., & Jayawardhana, R. 2012, *The Astrophysical Journal*, 745, 119. <http://adsabs.harvard.edu/abs/2012ApJ...745..119N>
- Nomura, H., & Millar, T. J. 2005, *Astronomy and Astrophysics*, 438, 923. <https://ui.adsabs.harvard.edu/abs/2005A%26A...438..923N/abstract>
- Oliphant, T. E. 2006 (Trelgol Publishing USA)
- Olofsson, J., van Holstein, R. G., Boccaletti, A., et al. 2018, *Astronomy & Astrophysics*, 617, A109. <https://www.aanda.org/10.1051/0004-6361/201832583>
- Olson, P. L., & Sharp, Z. D. 2019, *Physics of the Earth and Planetary Interiors*, 294, 106294. <http://adsabs.harvard.edu/abs/2019PEPI..29406294O>
- pandas development team, T. 2020, Zenodo. <https://doi.org/10.5281/zenodo.3509134>
- Parzen, E. 1962, *Ann. Math. Statist.*, 33, 1065. <https://projecteuclid.org/euclid.aoms/1177704472>
- Pearce, T. D., Krivov, A. V., & Booth, M. 2020, *Monthly Notices of the Royal Astronomical Society*, 498, 2798. <http://adsabs.harvard.edu/abs/2020MNRAS.498.2798P>
- Pedregosa, F., Varoquaux, G., Gramfort, A., et al. 2011, *Journal of Machine Learning Research*, 12, 2825
- Platt, J. C. 1999, in *Advances in Large Margin Classifiers* (MIT Press), 61–74
- Pontoppidan, K. M., Blake, G. A., van Dishoeck, E. F., et al. 2008, *The Astrophysical Journal*, 684, 1323. <https://ui.adsabs.harvard.edu/abs/2008ApJ...684.1323P/abstract>
- Ribas, Á., Macías, E., Espaillat, C. C., & Duchêne, G. 2018, *The Astrophysical Journal*, 865, 77. <http://adsabs.harvard.edu/abs/2018ApJ...865...77R>
- Riviere-Marichalar, P., Pinte, C., Barrado, D., et al. 2013, *Astronomy & Astrophysics*, 555, A67. <http://www.aanda.org/10.1051/0004-6361/201321506>
- Roberge, A., & Weinberger, A. J. 2008, *The Astrophysical Journal*, 676, 509. <https://ui.adsabs.harvard.edu/abs/2008ApJ...676..509R/abstract>

- Rosenblatt, M. 1956, *Ann. Math. Statist.*, 27, 832.
<https://projecteuclid.org/euclid.aoms/1177728190>
- Salyk, C., Blake, G. A., Boogert, A. C. A., & Brown, J. M. 2011, *The Astrophysical Journal*, 743, 112. <https://ui.adsabs.harvard.edu/2011ApJ...743..112S/abstract>
- Schindhelm, E., France, K., Herczeg, G. J., et al. 2012, *The Astrophysical Journal Letters*, 756, L23.
<http://adsabs.harvard.edu/abs/2012ApJ...756L..23S>
- Schöfer, P., Jeffers, S. V., Reiners, A., et al. 2019, *Astronomy and Astrophysics*, 623, A44.
<http://adsabs.harvard.edu/abs/2019A%26A...623A..44S>
- Schwarz, K. R., Bergin, E. A., Cleeves, L. I., et al. 2019, *The Astrophysical Journal*, 877, 131. <https://ui.adsabs.harvard.edu/2019ApJ...877..131S/abstract>
- Seok, J. Y., & Li, A. 2017, *ApJ*, 835, 291. <https://ui.adsabs.harvard.edu/abs/2017ApJ...835..291S/abstract>
- Spitzer, L. 1978, A Wiley-Interscience Publication. <https://ui.adsabs.harvard.edu/abs/1978ppim.book.....S/abstract>
- Takeuchi, T., & Artymowicz, P. 2001, *ApJ*, 557, 990.
<https://ui.adsabs.harvard.edu/abs/2001ApJ...557..990T/abstract>
- Theissen, C. A., & West, A. A. 2014, *The Astrophysical Journal*, 794, 146.
<http://adsabs.harvard.edu/abs/2014ApJ...794..146T>
- Tonry, J., & Davis, M. 1979, *The Astronomical Journal*, 84, 1511.
<http://adsabs.harvard.edu/abs/1979AJ.....84.1511T>
- Torres, C. A. O., Quast, G. R., da Silva, L., et al. 2006, *Astronomy and Astrophysics*, 460, 695
- Trapman, L., Miotello, A., Kama, M., van Dishoeck, E. F., & Bruderer, S. 2017, *A&A*, 605, A69.
<http://www.aanda.org/10.1051/0004-6361/201630308>
- Valenti, J. A., Johns-Krull, C. M., & Linsky, J. L. 2000, *The Astrophysical Journal Supplement Series*, 129, 399.
<http://stacks.iop.org/0067-0049/129/i=1/a=399>
- Van Der Walt, S., Colbert, S. C., & Varoquaux, G. 2011, *Computing in Science & Engineering*, 13, 22
- Virtanen, P., Gommers, R., Oliphant, T. E., et al. 2019, *arXiv:1907.10121 [physics]*.
<https://arxiv.org/abs/1907.10121>
- Webb, R. A., Zuckerman, B., Platais, I., et al. 1999, *The Astrophysical Journal Letters*, 512, L63.
<http://cdsads.u-strasbg.fr/abs/1999ApJ...512L..63W>
- Weidenschilling, S. J. 1977, *Monthly Notices of the Royal Astronomical Society*, 180, 57. <https://ui.adsabs.harvard.edu/#abs/1977MNRAS.180..57W/abstract>
- Weinberger, A. J., Becklin, E. E., Zuckerman, B., & Song, I. 2004, *The Astronomical Journal*, 127, 2246. <https://ui.adsabs.harvard.edu/abs/2004AJ....127.2246W/abstract>
- Weintraub, D. A., Kastner, J. H., & Bary, J. S. 2000, *The Astrophysical Journal*, 541, 767.
<http://adsabs.harvard.edu/abs/2000ApJ...541..767W>
- Wenger, M., Ochsenbein, F., Egret, D., et al. 2000, *Astronomy and Astrophysics Supplement Series*, 143, 9.
<http://adsabs.harvard.edu/abs/2000A%26AS..143...9W>
- Williams, J. P., & Cieza, L. A. 2011, *Annual Review of Astronomy and Astrophysics*, 49, 67
- Wood, B. E., Karovska, M., & Raymond, J. C. 2002, *The Astrophysical Journal*, 575, 1057. <https://ui.adsabs.harvard.edu/abs/2002ApJ...575.1057W/abstract>
- Wright, E. L., Eisenhardt, P. R. M., Mainzer, A. K., et al. 2010, *The Astronomical Journal*, 140, 1868.
<http://adsabs.harvard.edu/abs/2010AJ....140.1868W>
- Wyatt, M. C. 2008, *Annual Review of Astronomy and Astrophysics*, 46, 339. <http://adsabs.harvard.edu/abs/2008ARA%26A..46..339W>
- Yang, H., Johns-Krull, C. M., & Valenti, J. A. 2008, *The Astronomical Journal*, 136, 2286. <https://ui.adsabs.harvard.edu/abs/2008AJ....136.2286Y/abstract>
- Yang, H., Herczeg, G. J., Linsky, J. L., et al. 2012, *The Astrophysical Journal*, 744, 121. <https://ui.adsabs.harvard.edu/abs/2012ApJ...744..121Y/abstract>
- Youdin, A. N., & Goodman, J. 2005, *The Astrophysical Journal*, 620, 459.
<http://adsabs.harvard.edu/abs/2005ApJ...620..459Y>
- Youngblood, A., Pineda, J. S., & France, K. 2021, *The Astrophysical Journal*, 911, 112.
<https://ui.adsabs.harvard.edu/abs/2021ApJ...911..112Y>
- Youngblood, A., France, K., Loyd, R. O. P., et al. 2016, *The Astrophysical Journal*, 824, 101.
<http://adsabs.harvard.edu/abs/2016ApJ...824..101Y>